NOAA Technical Report ERL 431–WPL 61

Remote Sensing of Meteorological Parameters With the Aid of a Clear-Air Doppler Radar

Nandini Sengupta, James M. Warnock,
Earl E. Gossard, Richard G. Strauch

June 1987

U.S. DEPARTMENT OF COMMERCE
National Oceanic and Atmospheric Administration
Environmental Research Laboratories

NOAA Technical Report ERL 431–WPL 61

Remote Sensing of Meteorological Parameters With the Aid of a Clear-Air Doppler Radar

Nandini Sengupta
Wave Propagation Laboratory

James M. Warnock
Aeronomy Laboratory

Earl E. Gossard
Cooperative Institute for Research in the
Environmental Sciences (CIRES)

Richard G. Strauch
Wave Propagation Laboratory

Wave Propagation Laboratory
Boulder, Colorado

June 1987

U.S. Department of Commerce
Malcolm Baldrige, Secretary

National Oceanic and Atmospheric Administration
Anthony J. Calio, Administrator

Environmental Research Laboratories
Boulder, Colorado
Vernon E. Derr, Director

CONTENTS

Remote Sensing of Meteorological Parameters With the Aid of a Clear-Air Doppler Radar

N. Sengupta, J.M. Warnock[1], E.E. Gossard[2], R.G. Strauch

ABSTRACT. The described experiment tested the feasibility of (a) using a surface-based radar to measure gradients of temperature and humidity aloft and (b) using standard radiosonde data to calculate height profiles of the radio refractive index structure parameter, C_n^2. The experiment employed the WPL wind-profiling radar (915 MHz) at Stapleton Field, Denver, Colorado, operated in a special dedicated mode. The radar measured backscattered power and Doppler wind spectra from which C_n^2, Doppler spectral width, and turbulent dissipation rate ε were calculated. From these quantities the ratio $C_n^2/\varepsilon^{2/3}$ was calculated and used to deduce temperature and refractive index gradient values for comparison with the raob-measured values. The statistical model developed by NOAA's Aeronomy Laboratory was used to calculate values of C_n^2 and ε for comparison with the radar-measured values. The agreement between the radar-calculated and observed quantities and the in situ balloon-observed quantities was as good as could be expected considering the temporal variability of the layer structure and the spatial displacement of the balloon/radar soundings. However, clouds were found to be an important source of errors and ambiguities in interpretation.

1. INTRODUCTION

For more than a decade, sensitive pulse Doppler radars operating at VHF and UHF have been used to probe the clear air in the boundary layer (e.g., James, 1980) and through the troposphere and lower stratosphere (e.g., Green et al., 1975; Harper and Gordon, 1980). It is well established that these radars can measure vertical profiles of the horizontal and vertical wind in the clear air (e.g., Chadwick et al., 1976; Warnock et al., 1978; Fukao et al., 1982; Clark et al., 1985; Strauch et al., 1986). Many of these radars were designed and built specifically to measure the wind, and are sometimes called wind profilers. Further, networks of these radars can now operate routinely to provide continuous measurement of the wind with excellent time and height resolution (e.g., Strauch et al., 1984).

In addition to the mean Doppler shift from which wind measurements are deduced, the Doppler spectra contain a wealth of information on the scattering region. Since clear-air radars detect echoes from fluctuations in the refractive index caused by turbulent mixing of the radio refractivity, the total echo power is proportional to the refractivity turbulence structure parameter, and the Doppler spectral width is related to the turbulent dissipation rate.

The incentives behind the present investigation were twofold: (1) To test the feasibility of using radar profiler measurements of the structure constant C_n^2 and the Doppler velocity spectral width to aid in the retrieval of temperature gradients in elevated layers. (Therefore, in this study the radar-deduced gradients are compared with the radiosonde (raob) measured gradients.) (2) To

[1]NOAA/Aeronomy Laboratory, Boulder, Colorado 80303

[2]Cooperative Institute for Research in the Environmental Sciences (CIRES), University of Colorado/ NOAA, Boulder, Colorado 80309

test the Aeronomy Laboratory model for calculating profiles of the structure constant C_n^2 from given radiosonde mean gradient data.

Backscattered power, spectral width, and wind speed and direction data were obtained from the Wave Propagation Laboratory's UHF wind-profiling radar (see Strauch et al., 1984) at Stapleton Airport, Denver. In this experiment the radar was usually operated in its highest time and space resolution mode for 1 h following the raob launch. The launch site is located next to the radar.

2. THEORETICAL BACKGROUND OF THE EXPERIMENT

2.1 Some Elementary Turbulence Relationships

Some relatively simple relationships between radar-measurable quantities and atmospheric conditions of static stability and shear can be derived if it is assumed that the inertial subrange exists over the turbulence scales sensed by the radar. For example in homogeneous isotropic turbulence, the one-dimensional velocity and temperature spectra are given, respectively, by (see any standard turbulence text)

$$S_v(k) = A\varepsilon^{2/3}k^{-5/3} = \frac{A}{B}C_v^2 k^{-5/3} \tag{1a}$$

and

$$S_\theta(k) = A_\theta \varepsilon^{-1/3}\varepsilon_\theta k^{-5/3} = \frac{A_\theta}{B_\theta}C_\theta^2 k^{-5/3} \quad , \tag{1b}$$

where k is wavenumber, ε is turbulent dissipation rate of kinetic energy, and ε_θ the dissipation of half-variance of temperature. A is a universal constant $\simeq$0.5 for the wind component parallel to the flow and $\simeq$0.68 for components perpendicular to it. $B = 4A$, and C_v^2 is the velocity structure parameter. A_θ and B_θ are universal constants equal to 0.8 and 3.2 and C_θ^2 is the temperature structure parameter. The energy balance equation and and the corresponding temperature variance balance equation for steady-state conditions can be written (e.g., Lumley and Panofsky, 1964):

$$\varepsilon = -\langle wu\rangle \frac{\partial V_0}{\partial z}(1 - R_f) \tag{2a}$$

$$\varepsilon_\theta = -\langle \theta w\rangle \frac{\partial \theta_0}{\partial z} \tag{2b}$$

where angle brackets denote average and where pressure covariance terms and divergence of variance flux are negligible. In (2), u and w are the perturbations of horizontal and vertical velocity respectively and θ is temperature perturbation; $\partial V_0/\partial z$ and $\partial\theta_0/\partial z$ are the gradients with height of the unperturbed horizontal velocity and unperturbed potential temperature. The flux Richardson number $R_f = \langle w\theta\rangle(\partial\theta_0/\partial z)/\langle uw\rangle(\partial V_0/\partial z) = (K_H/K_M)$ Ri, where Ri is the gradient Richardson number given by

$$\mathrm{Ri} = \frac{g}{\theta_0}\frac{\left(\frac{\partial\theta_0}{\partial z}\right)}{\left(\frac{\partial V_0}{\partial z}\right)^2} \equiv \frac{N^2}{S^2} \quad , \tag{3}$$

and $N = [(g/\theta_0)\,(d\theta_0/dz)]^{1/2}$ is the Brunt-Väisälä frequency, S is the vertical shear of the horizontal mean wind, and g is the acceleration of gravity. The eddy coefficients K_H and K_M are defined as $K_H = \langle w\theta\rangle(\partial\theta_0/\partial z)$ and $K_M = -\langle wu\rangle(\partial V_0/\partial z)$, so that (2) can be written (e.g., Ottersten, 1969)

$$K_M = \frac{\varepsilon}{\left(\frac{\partial V_0}{\partial z}\right)^2 (1 - R_f)} \quad . \tag{4}$$

Furthermore, turbulence similarity considerations lead to the conclusion that the temperature structure parameter C_θ^2 is related to the rate of dissipation of temperature half-variance ε_θ by (Corrsin, 1951)

$$C_\theta^2 = B_\theta \, \varepsilon^{-1/3} \, \varepsilon_\theta \quad . \tag{5}$$

Therefore, letting $B\varepsilon^{2/3} = C_v^2$ [see (1)], we obtain

$$C_\theta^2 = B_\theta \left(\frac{C_v^2}{B}\right)^{-1/2} \left(\frac{K_H}{K_M}\right) K_M \left(\frac{\partial \theta_0}{\partial z}\right)^2 \quad .$$

So, after (4) is used to eliminate K_M, these equations and definitions lead to the fundamental relationship between the velocity and temperature structure parameters and the velocity and temperature gradients; i.e.,

$$C_\theta^2 \left(\frac{\partial \theta_0}{\partial z}\right)^{-2} = \frac{B_\theta}{B} \left(\frac{K_M}{K_H} - \mathrm{Ri}\right)^{-1} \left[C_v^2 \left(\frac{\partial V_0}{\partial z}\right)^{-2}\right], \tag{6a}$$

where K_M/K_H is the term often called the turbulent Prandtl Number, Pr. Eliminating the shear by using (3), we readily see that

$$C_\theta^2 \left(\frac{g}{\theta_0} \frac{\partial \theta_0}{\partial z}\right) = \frac{B_\theta}{B} \left(\frac{\mathrm{Ri}}{\mathrm{Pr} - \mathrm{Ri}}\right) C_v^2 \left(\frac{\partial \theta_0}{\partial z}\right)^2 \quad . \tag{6b}$$

2.2 The Microwave Refractive Index

In the present experiment, radar is used as the remote-sensing device, and the Bragg scatter of electromagnetic waves is proportional to C_n^2 (where n is the radar refractive index) rather than C_θ^2, the quantity appearing in (1), (5), and (6) (e.g., Gossard and Strauch, 1983; Doviak and Zrnic, 1984). Therefore, it is necessary to relate the turbulent structure of the temperature field to that of the radar refractive index field.

The radio refractive index n at microwave frequencies is related to temperature, humidity, and pressure by (e.g., Bean and Dutton, 1966)

$$(n - 1) \times 10^6 = \frac{77.6P}{T} \left(1 + \frac{7.73Q}{T}\right) \quad , \tag{7}$$

where P is pressure in millibars, Q is the humidity mixing ratio in grams of moisture vapor per kilogram of dry air, and T is temperature in kelvins. We use the potential refractive index ϕ instead of n and θ instead of T, because both are conserved in adiabatic movements of air parcels and are therefore useful in analyzing turbulent effects. We define ϕ as the value of $(n-1) \times 10^6$ that a parcel would have if moved adiabatically to the 1000-mb level without gain or loss of moisture (no condensation or evaporation). Thus

$$\phi_t = \frac{77600}{\theta_t} \left(1 + \frac{7.73Q_t}{\theta_t}\right) \quad , \tag{8}$$

where θ is the potential temperature, given by

$$\theta + T(K) \left(\frac{1000}{P}\right)^{0.286} \quad ,$$

and the subscript t is used for total quantities, in order to avoid confusion with unperturbed average quantities (subscript zero), and perturbation quantities (see Sec. 2.4).

In the development analogous to that leading to (6), we find, assuming that $K_Q \equiv K_H$,

$$C_Q^2 = B_Q \left(\frac{C_v^2}{B}\right)^{-1/2}\left(\frac{K_Q}{K_M}\right) K_M \left(\frac{\partial Q_0}{\partial z}\right)^2 .$$

Whence, inserting (3), and assuming $K_H = K_Q$ and $B_\theta = B_Q$, we find

$$C_Q^2 = \frac{B_\theta}{B}\left(\frac{K_M}{K_H} - \mathrm{Ri}\right)^{-1}\left[C_v^2 \left(\frac{\partial V_0}{\partial z}\right)^{-2}\right]\left(\frac{\partial Q_0}{\partial z}\right)^2 . \tag{9}$$

Similarly, assuming $K_H = K_Q = K_\phi$ and $B_\theta = B_Q = B_\phi$

$$C_\phi^2 N^2 = \frac{B_\theta}{B}\,\mathrm{Ri}\,(\mathrm{Pr} - \mathrm{Ri})^{-1}\, C_v^2\left(\frac{\partial \phi_0}{\partial z}\right)^2 . \tag{10}$$

So in (6)–(10) we have expressed the ratio of turbulent quantities in terms of mean gradient quantities.

2.3 Relationships of Structure Parameters to Length Scales and Mean Gradients

Equations (6) and (9) can be expressed in terms of a vertical length scale L as follows (see Tatarskii, 1971, p. 72; Gossard et al., 1984). ***Random differences*** relative to position in a homogeneously turbulent inertial subrange lead to

$$\langle[\theta(r) - \theta(r+\ell)]^2\rangle = C_\theta^2\, \ell^{2/3} \tag{11a}$$

$$\langle[V(r) - V(r+\ell)]^2\rangle = C_w^2\, \ell^{2/3} \tag{11b}$$

for mean square differences measured at two points separated (say vertically) by the distance ℓ. On the other hand, if mean vertical gradients of θ (or vector velocity $\mathbf{V}$) exist, the difference in (say) θ at two points vertically separated by distance ℓ is $\ell\,(\partial\theta_0/\partial z)$ so that the mean square difference resulting from mixing in the presence of this type of ***systematic difference*** in position is

$$\langle[\theta(z) - \theta(z+\ell)]^2\rangle = \ell^2\,(\partial\theta_0/\partial z)^2 \tag{12a}$$

$$\langle[V(z) - V(z+\ell)]^2\rangle = \ell^2\,(\partial V_0/\partial z)^2 \tag{12b}$$

For small differences, the contribution to the variance from the random difference due to position given by (11) will dominate, but for larger scales the contribution due to the systematic difference with height given by (12) becomes dominant, so that a scale L can be defined for which the two contributions are just equal. Then $C_\theta^2 L_\theta^{2/3} = (\partial\theta_0/\partial z)^2 L_\theta^2$, so

$$L_\theta^{4/3} = \frac{C_\theta^2}{\left(\frac{\partial\theta_0}{\partial z}\right)^2} , \qquad L_v^{4/3} = \frac{C_v^2}{\left(\frac{\partial V_0}{\partial z}\right)^2} , \tag{13a,b}$$

and similar reasoning leads to the conclusion that

$$L_Q^{4/3} = \frac{C_Q^2}{\left(\frac{\partial Q_0}{\partial z}\right)^2} \quad , \qquad L_\phi^{4/3} = \frac{C_\phi^2}{\left(\frac{\partial \phi_0}{\partial z}\right)^2} \quad , \tag{14a,b}$$

where Q is the humidity mixing ratio. Experiments show (Gossard et al., 1984) that L_Q and L_θ are equal, or very nearly so, but that L_v may differ substantially from the others. Theoretically, if $L_Q = L_\theta$, then $L_\phi = L_Q = L_\theta$, which is borne out by the above referenced experiments. The above development implicitly assumes that the ⅔ law holds as ℓ increases out to the value L. (Tatarskii therefore adopted L_v as a definition of the outer scale L_0.) Then, noting that $\varepsilon = (C_v^2/B)^{3/2}$ [see (1a)], we find

$$\varepsilon = L_0^2 \, (\partial V_0/\partial z)^3 \quad , \tag{15}$$

where we have absorbed the constant in the definition of L_0.

From (6), (13), and (14a), it is clear that similar scales can be defined for temperature and humidity; i.e.,

$$\begin{aligned} L_{0\theta} &= \left\{ \frac{B_\phi}{B} \left(\frac{K_M}{K_H} - \mathrm{Ri} \right)^{-1} \left[C_v^2 \left(\frac{\partial V_0}{\partial z} \right)^{-2} \right] \right\}^{3/4} \\ &= \left[\frac{B_\phi}{B} \left(\frac{K_M}{K_H} - \mathrm{Ri} \right)^{-1} \right]^{3/4} L_{0v} = L_{0Q} \quad . \end{aligned} \tag{16}$$

It is necessary to qualify the above derivation because the ***vertical*** velocity component, w, will be the convenient one to measure in the radar experiment, whereas in the development leading to (15) it is implicitly assumed that V and V_0 were ***horizontal*** components of the wind. Therefore, to justify the substitution of w for V in (12b), we must assume that the redistribution of momentum among velocity components takes place fast enough that isotropy essentially exists for those scales important to whatever experiment is being run. However, none of the hypotheses tested in this report requires the use of (12b) or (13b) except the testing of (15).

In the present experiments the relationships (6), (9), and (15) are evaluated as reliable indicators of the relationship between atmospheric gradients and various turbulent quantities capable of being sensed by radars.

Some form of (6) has been used by several workers [e.g., VanZandt et al. (1978); Gage et al. (1980), Gossard et al. (1982), and Warnock and VanZandt (1985)] assuming (unrealistically) constant values for the Prandtl number, $\mathrm{Pr} = K_M/K_H$, and Ri. The basic approach leading to (6) was in fact initiated by Ottersten (1969). In spite of the unrealistic assumption that Pr and Ri were constants, this approach has generally led to good agreement between the radar observations of C_ϕ^2 and the raob-measured or tower-measured values of the mean gradients of temperature and humidity that determine the refractive index gradients. An explanation of this paradox was proposed by Gossard and Frisch (1987) who found, by combining results from analysis of the heat flux equation and the kinetic energy balance equation, that Ri/(Pr − Ri) should be essentially constant; that is,

$$C = \frac{B}{B_\theta} \frac{(\mathrm{Pr} - \mathrm{Ri})}{\mathrm{Ri}}$$

over a range of Ri from about 0.1 to 1.0. Equation (16) then gives

$$\frac{\partial \theta_0}{\partial z} = C \frac{g}{\theta_0} \frac{C_\theta^2}{C_w^2} = \frac{C}{2.7} \frac{g}{\theta_0} \frac{C_\theta^2}{\varepsilon^{2/3}} \quad . \tag{17}$$

From a regression analysis of temperature and velocity variance data recorded with platinum wire and sonic anemometer sensors on the 300-m tower of the Boulder Atmospheric Observatory, it has been found (Gossard and Frisch, 1987) that $C \simeq 2.2$.

2.4 The Refractive Index Perturbation Equations

We wish to infer information about temperature and humidity gradients from the radar measurements of $C_\phi^2/\varepsilon^{2/3}$. However (17) provides only a relationship between temperature gradient and $C_\theta^2/\varepsilon^{2/3}$. We must therefore relate the gradients $\partial\theta_0/\partial z$ and $\partial Q_0/\partial z$ to $C_\phi^2/\varepsilon^{2/3}$.

Because the turbulent perturbations of temperature are small compared with the average value, (8) shows that perturbations in refractive index can be accurately expressed by

$$\phi \simeq -a\theta + bQ \quad , \tag{18}$$

where, now, the deviation from the average is unsubscripted, and the subscript "0" is the unperturbed average quantity as before. From (8) and (18) we see that

$$a = \frac{77600}{\theta_0} \left(\frac{1}{\theta_0} + 15.46 \frac{Q_0}{\theta_0^2} \right) \quad , \qquad b = 77600 \left(\frac{7.73}{\theta_0^2} \right)$$

so that

$$\langle \phi^2 \rangle = a^2 \langle \theta^2 \rangle + b^2 \langle Q^2 \rangle - 2ab \langle \theta Q \rangle \quad . \tag{19}$$

The importance of the cross-covariance term in calculating the magnitude of the refractive index variance and power spectrum was first pointed out by Gossard (1960). From (19) it follows that

$$C_\phi^2 = a^2 C_\theta^2 + b^2 C_Q^2 - 2abR\sqrt{C_\theta^2 C_Q^2} \quad ,$$

where R is the correlation coefficient between temperature and humidity. Within the error of measurement by tower-borne sensors of temperature and humidity, it was shown by Gossard et al. (1984) that the correlation of θ and Q within stable layers is very high and that $L_\theta = L_Q$ [see (12) and (13)], so that

$$\frac{C_Q^2}{\left(\frac{\partial Q_0}{\partial z}\right)^2} = \frac{C_\theta^2}{\left(\frac{\partial \theta_0}{\partial z}\right)^2} = \frac{C_\phi^2}{\left(\frac{\partial \phi_0}{\partial z}\right)^2} \quad . \tag{20a}$$

The first equality is rigorously true if Q and θ are perfectly correlated. Equation (20a) can then be written

$$C_\phi^2 = C_\theta^2 \left[a^2 + b^2 \frac{\left(\frac{\partial Q_0}{\partial z}\right)^2}{\left(\frac{\partial \theta_0}{\partial z}\right)^2} - 2ab \frac{\left(\frac{\partial Q_0}{\partial z}\right)}{\left(\frac{\partial \theta_0}{\partial z}\right)} \right] \quad . \tag{20b}$$

Using (17) to eliminate C_θ^2, in (20a) or (20b) we have expressions relating the measurable ratio $C_\phi^2/\varepsilon^{2/3}$ to the gradients of refractive index or of temperature and humidity; i.e., we find the quadratic equation for $\partial\theta_0/\partial z$:

$$\left(\frac{\partial\theta_0}{\partial z}\right)^2 - \left[2\,\frac{b}{a}\,R\,\frac{\partial Q_0}{\partial z} + \frac{C}{2.7\,a^2}\left(\frac{g}{\theta_0}\right)\frac{C_\phi^2}{\varepsilon^{2/3}}\right]\frac{\partial\theta_0}{\partial z} + \frac{b^2}{a^2}\left(\frac{\partial Q_0}{\partial z}\right)^2 = 0 \quad . \tag{21}$$

At the 700-mb average altitude of the sounding data above Denver, Colorado, a typical potential temperature is 315 K, and $a \simeq 0.82$, $b \simeq 6.05$. Furthermore, it was shown by Gossard et al. (1984), from tower data collected within a stable layer, that the magnitude of the correlation (positive or negative depending on the relative gradients) between humidity and temperature fluctuations is very high under statically stable conditions. In fact in that study the coherence remained above 0.85 out to the highest frequency measurable by the sensors (5 Hz). Figure 1 shows a plot of the solution of (21), if we choose $R \simeq 1$, and use the values of a and b stated above for Denver at 700 mb.

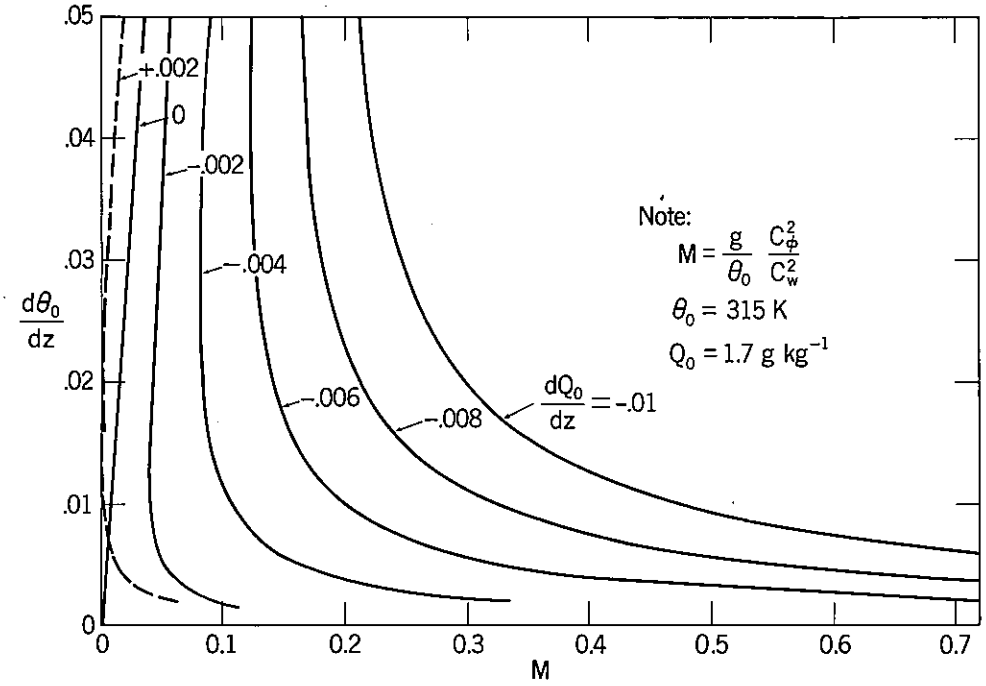

Figure 1. Plot of $d\theta_0/dz$ vs. M [where $M = (g/\theta_0)\,(C_\phi^2/C_w^2) \equiv (g/2.7\theta_0)\,(C_\phi^2/\varepsilon^{2/3})$], parametric in dQ_0/dz.

If knowledge of the mean humidity gradient is available from an independent source, such as raob, radar measurements of $C_\phi^2/\varepsilon^{2/3}$ can be used to calculate $d\theta_0/dz$ and compare it with raob data, or, alternatively, from (17) and (20a), to calculate $d\phi_0/dz$ if a temperature gradient is available.

2.5 Aeronomy Laboratory Model for Calculating $C_n^2(C_\phi^2)$ and ε

In recent years a model has been developed to estimate C_ϕ^2 and ε in the clear air from height profiles of air pressure P, temperature T, relative humidity, and horizontal wind speed and direction (VanZandt et al., 1978, 1981; Warnock and VanZandt, 1985; Warnock et al., 1985). The basic concept of the model is that the wind, potential temperature, and humidity and their vertical gradients fluctuate about their mean values. Since Ri depends on the wind shear and potential temperature gradient, it also fluctuates about its mean value. At scales much smaller than can be observed by the raob, these fluctuations may occasionally produce a value of $\mathrm{Ri} \leq \mathrm{Ri_c}$, its critical value for the onset of turbulence; therefore a turbulent layer may form. This layer will mix the existing refractive index structure to produce fluctuations in the refractive index. It is these fluctuations that are sensed by remote sensors such as the Stapleton radar.

2.5.1 Model input data

The in situ data used in this study are routine NWS raob data. The raob balloons were launched at Stapleton International Airport from a location near WPL's Stapleton radar. The best height resolution of T, P, and relative humidity that can be obtained from a standard raob instrument is about 150 m. During routine NWS operations, however, not every measurement is analyzed. Instead the data are analyzed only where there is a significant change in the height gradient of the temperature or humidity, and at certain mandatory pressure levels. Thus, the temperature and humidity profiles are a linear piecewise approximate fit to the raw data with a height resolution of 150 m at best. Winds are measured and the data analyzed for every minute during the balloon flight. Since the ascent rate of a typical balloon flight is about 5 m s^{-1}, the wind measurements are separated by about 300 m.

The first step in analyzing the balloon data for input into the model calculations is to compute the potential temperature θ, the specific humidity q = ratio of mass of water vapor to mass of moist air, and the vector wind $\mathbf{V}$. For notational simplicity, we have dropped the zero subscript. Next, we compute parameters that depend on the vertical gradients of the variables θ, q, and $\mathbf{V}$. The gradients of θ and $\mathbf{V}$ with height are defined in terms of N and S [see (3)], and $q' = \partial q/\partial z$.

2.5.2 Mean values of a slab of the atmosphere

To calculate these height derivatives we consider a slab of the atmosphere that is determined by two consecutive balloon measurements of a variable. Thus the thinnest T or relative humidity slab would be about 150 m, but some slabs are more than 1 km thick, whereas the wind slabs are about 300 m thick unless part of the wind data series is missing. Next the gradients are obtained by differencing linearly the measured values. We use an overbar to denote a slab variable.

One of the fundamental assumptions of the model is that T, q, and $\mathbf{V}$ fluctuate about their mean values on scales much smaller than can be measured using standard instruments such as raobs. These fluctuations, of course, produce fluctuations in their gradients and, therefore, in N^2, q', and S and also in $\mathrm{Ri} = N^2/S^2$ [see (3)]. We call these small-scale fluctuations about the mean value of the slab "fine structure." A second basic assumption of the model is that the shear flow becomes dynamically unstable where the local fine structure value of Ri becomes less than a critical value $\mathrm{Ri_c}$ so that thin horizontally stratified turbulent layers are formed.

2.5.3 Turbulent layers

For an individual turbulent layer, which we label by its values of outer scale L_0, C_ϕ^2 and ε are (Tatarskii, 1971)

$$C_\phi^2 = 2.8\ M^2\ L_0^{4/3} \tag{22}$$

$$\varepsilon = S^3\ L_0^2 \quad , \tag{23}$$

assuming that the turbulence is stationary in time, homogeneous, and isotropic [see (14b) and (15)]. In (22), M is the vertical gradient of the generalized potential refractive index for the turbulent layer (Ottersten, 1969; Tatarskii, 1971) given by

$$M = C_2 \frac{P}{T} \frac{N^2}{g} \left(1 + C_3 \frac{q}{T} - \frac{C_3}{2} \frac{q'/T}{N^2/g} \right) \quad ,$$

where the constants C_2 and C_3 are -77.6×10^{-6} and 15500, respectively, and g is the acceleration of gravity. [See Sec. 2.3 for a complete discussion of the assumptions inherent in (22) and (23)]. Note that C_ϕ^2 depends on two things. First, there must be a turbulence flow with an intensity described by ε; second, there must be a refractive index gradient (which is described by M) that is mixed by the turbulent flow.

2.5.4 Mean values of C_ϕ^2 and ε for a slab

Next we estimate the mean values of C_ϕ^2 and ε for an entire slab ($\overline{C_\phi^2}$ and $\bar{\varepsilon}$). Ideally, if we had sufficient fine-scale data including measurements of the inertial subrange fluctuation, we could calculate the values of both variables for each turbulent layer in the slab. Then we could simply compute the mean values of C_ϕ^2 and ε for the slab. In practice, of course, there are never sufficient data available to calculate C_ϕ^2 and ε for each layer throughout the entire atmosphere, so we are forced to use a probabilistic approach. In this approach we consider the probability of a value of the parameters anywhere in the slab. We can think of this procedure as having two parts; one part is to estimate the probability of occurrence of turbulence, and the second part is to weight this probability appropriately by the layer values for C_ϕ^2 and ε given in (22) and (23), respectively.

To estimate the probability of a layer with outer scale L_0, consider a plane with N^2 as the ordinate and S^2 as the abscissa. Since $\mathrm{Ri} = N^2/S^2$, each point is the plane has a unique value of Ri. As discussed above, the fine-scale fluctuations in N^2 and S^2 about their mean values produce fluctuations in Ri. Where the value of $\mathrm{Ri} \le \mathrm{Ri}_c$, the turbulent layers are formed. We have found that we can estimate C_ϕ^2 accurately, and have a deterministic solution to the model by estimating the fluctuations of N^2 and S^2 about their mean values in terms of the mean observable quantities of the slab and L_0. Thus, in the model the fluctuation of Ri for a given L_0 depends only on the balloon data. In the earlier versions of the model (VanZandt et al., 1978; Gage et al., 1978), L_0 was taken as an adjustable parameter. A value of $L_0 = 10$ m was found to give satisfactory agreement with the data. In later versions of the model (VanZandt et al., 1981; Warnock et al., 1985; Warnock and VanZandt, 1985) we have assumed a distribution of L_0's, and integrated over a range of L_0 values. Thus we have

$$\overline{C_\phi^2} = \int_{L_{min}}^{L_{max}} dL \iint_{\mathrm{Ri} \le \mathrm{Ri}_c} dS\ dN^2 \int_{-\infty}^{+\infty} dq'\ p_4\ C_\phi^2 \tag{24}$$

and

$$\bar{\varepsilon} = \int_{L_{min}}^{L_{max}} dL \iint_{\mathrm{Ri} \le \mathrm{Ri}_c} dS\ dN^2 \int_{-\infty}^{+\infty} dq'\ p_4\ \varepsilon \quad , \tag{25}$$

where p_4 is the multivariate probability density function for a point in a layer with outer scale between L_0 and $L_0 + dL_0$; we have shear between S and $S + dS$, stability between N^2 and $N^2 + dN^2$, and humidity gradient between q' and $q' + dq'$. Note that the limits on the integrals restrict the integration over the $N^2 - S$ plane to the region where $\mathrm{Ri} \le \mathrm{Ri}_c$. To date we have used $\mathrm{Ri}_c = \frac{1}{4}$, but the program is designed to adjust the value easily.

Next we simplify p_4 by factoring it into four univariate probability density functions, p_L, p_N, p_S, $p_{q'}$. We can further simplify the integrals by noting the high correlation or anticorrelation between the fine-scale fluctuations in q' and N^2 relative to their mean values (e.g., see Fig. 7 of Gossard et al., 1984), so that

$$\frac{q'}{(\overline{q'})} = \pm \frac{N^2}{\overline{N^2}} \quad . \tag{26}$$

With this relation, $C_\phi{}^2$ in (24) is independent of q' so that (24) and (25) can be written as

$$\overline{C_n^2} = 2.8 \int_{L_{\min}}^{L_{\max}} dL\ p_L\ L^{4/3} \int_0^{\infty} dS\ p_S \int_{-\infty}^{S^2\mathrm{Ri}_c} dN^2\ p_N\ M^2 \int_{-\infty}^{+\infty} dq'\ p_{q'} \tag{27}$$

$$\overline{\varepsilon} = \int_{L_{\min}}^{L_{\max}} dL\ p_L\ L^2 \int_0^{\infty} dS\ p_S\ S^3 \int_{-\infty}^{S^2\mathrm{Ri}_c} dN^2\ p_N \int_{-\infty}^{+\infty} dq'\ p_{q'} \quad . \tag{28}$$

Since the inner integral over q' is unity by definition, (27) and (28) become

$$\overline{C_n^2} = 2.8 \int_{L_{\min}}^{L_{\max}} dL\ p_L\ L^{4/3} \int_0^{\infty} dS\ p_S \int_{-\infty}^{S^2\mathrm{Ri}_c} dN^2\ p_N\ M^2 \tag{29}$$

$$\overline{\varepsilon} = \int_{L_{\min}}^{L_{\max}} dL\ p_L\ L^2 \int_0^{\infty} dS\ p_S\ S^3 \int_{-\infty}^{S^2\mathrm{Ri}_c} dN^2\ p_N \quad . \tag{30}$$

Next we specify the probability density functions (pdf's). Because of the lack of a complete knowledge on the production of turbulence and the scarcity of fine-scale observations, we have considerable latitude in choosing both the form and parameters of the pdf's. In fact the exact form of a pdf is less important than accurate estimates of parameters. Thus we choose the simplest form that is consistent with observations. In addition all the parameters of the distributions must be given in terms of the observed large-scale data and L_0.

For L_0 we use a uniform distribution:

$$p_L = \text{constant} \, . \tag{31}$$

The constant is chosen so that

$$\int_{L_{min}}^{L_{max}} p_L \, dL = 1.0 \quad . \tag{32}$$

For the vector shear S we choose a Rice-Nakagami distribution (e.g., Beckmann, 1967). This distribution is obtained when both components of the vector shear are Gaussian distributed with a standard deviation σ_S common to the fluctuations of both components. It is given by

$$p_S = \frac{S}{\sigma_S^2} \exp - \left(\frac{S^2 + \overline{S^2}}{2 \, \sigma_S^2} \right) \, I_0 \left(\frac{S \, \bar{S}}{\sigma_S^2} \right) \, , \tag{33}$$

where

$$\sigma_S = \sigma_1 \, L^{\alpha_L} \overline{N^2}^{\alpha_N} \rho^{\alpha_\rho} \, , \tag{34}$$

and $\sigma_1 = 0.18$ is chosen to be consistent with observations, $\alpha_L = -0.3$, $\alpha_N = ¼$, $\alpha_\rho = -0.15$, and ρ is the density.

For the stability pdf, we use a Gaussian distribution:

$$p_N = \frac{1}{\sqrt{2\pi} \, \sigma_N} \exp - \left[\frac{(N^2 - \overline{N^2})^2}{2 \, \sigma_N^2} \right] \, , \tag{35}$$

where σ_N is the standard deviation of the distribution, given by

$$\sigma_N = \sqrt{6/5} \, \sigma_S \, \overline{N^2}^{1/2} \quad . \tag{36}$$

The model is now completely specified. We use the numerical integration techniques described by Warnock and VanZandt (1985) to compute the estimates of $\overline{C_\phi^2}$ and $\bar{\varepsilon}$.

2.6 Radar Measurements

From radar measurements, $C_\phi^2/\varepsilon^{2/3}$ can be calculated from the magnitude of the backscattered power and the width of the Doppler spectrum. That is, from the Doppler spectral width the radar can (in principle) measure ε, and from the backscattered power the radar can measure C_ϕ^2.

C_ϕ^2 is found from the relationship (e.g., Doviak and Zrnic, 1984; Gossard and Strauch, 1983, Ch. 12 and Appendix A)

$$C_\phi^2 = C_n^2 = \frac{337 \, \ln 2 \, \lambda^{1/3}}{\pi \, A_e \, \Delta} \, \frac{R^2}{P_t} \, P_r \, , \tag{37}$$

where P_r is the received power (W) and P_t is the power transmitted (W), A_e is the effective antenna aperture (m^2), Δ is the pulse length (m), and R is the range (m).

A radar-estimated value of ε can be calculated from the method of Frisch and Clifford (1974) as described by Gossard and Strauch (1983, Ch. 7, p. 145 and Appendix D). Thus, it is found that

$$\varepsilon = \delta^{-1}\left[\frac{\sigma_{11}^{\,2}}{2.16\left(1-\frac{\gamma^2}{15}\right)}\right]^{3/2}. \tag{38}$$

If $b \le a$, $\delta = a$ and $\gamma^2 = 1-(b/a)^2$; and if $b > a$, $\delta = b$ and $\gamma^2 = 4[1-(a/b)^2]$; $\sigma_{11}^{\,2}$ is the variance of the radar Doppler velocity spectrum and (here only) a and b are (Gaussian) beamwidth and (Gaussian) pulse length respectively. The methods of calculating the appropriate moments from the Doppler spectra are described in Gossard and Strauch (1983, Ch. 11).

Equations (37) and (38) were used to calculate $C_\phi^{\,2}$, ε, and the ratio $C_\phi^{\,2}/\varepsilon^{2/3}$ from the radar data described in Sec. 3.2.

3. EXPERIMENT RESULTS

3.1 Radar Characteristics

The 915-MHz (UHF) wind-profiling radar of the Wave Propagation Laboratory has been in operation since February 1983 near Stapleton Airport, Denver. Table 1 lists characteristics and operating parameters of the radar.

The radar was operated, for most of the experiment, in its highest time- and space-resolution mode with antenna pointing in the zenith direction for approximately 1 h after the morning raob launch.

Table 1a. — Stapleton radar characteristics

Frequency	915 MHz
Maximum bandwidth	2 MHz
Peak power	5.6 kW
Duty cycle	<25%
Antenna aperture	≈10 m × 10 m
Antenna pointing	Zenith, 15° off-zenith to north and east
Antenna type	Offset paraboloidal reflector with offset horn feeds
Two-way beamwidth	1.7°
System noise temperature	240 K

Table 1b. — Stapleton radar operating parameters

	Normal mode			Special mode*
	1	2	3	
Data Processing				
Pulse width	1 μs	3 μs	9 μs	1 μs
Pulse repetition period	50 μs	64 μs	110 μs	50 μs
Average power	110 W	260 W	450 W	110 W
Time domain averaging	136 pulses	80 pulses	46 pulses	136 pulses
Spectral averaging	8 spectra	32 spectra	32 spectra	11 spectra
Maximum radial velocity	±12.02 m/s	±15.97 m/s	±16.16 m/s	±6 m/s
Spectral resolution (64 points)	0.376 m/s	0.499 m/s	0.505 m/s	0.188 m/s
Height sampling				
First height	0.35 km	1.64 km	2.7 km	0.35 km
Height spacing	100 m	290 m	870 m	150 m
Number of heights	24	24	18	24

*Rapid-sampling, vertically pointing, 1-μs pulses.

3.2 Case Studies

3.2.1 20 July 1986

The temperature profile obtained from the raob on 20 July 1986 around 1200 GMT showed a temperature inversion at about 2.7 km. During this period the radar antenna was pointing north (15° off zenith) and east (15° off zenith) and then held in the vertical direction for 1 h, obtaining profiles of raw spectra every 30 s. Backscattered power, Doppler vertical velocity, and Doppler spectral width were then computed from these spectra. At the end of the hour, the antenna was again pointed east and then north so that horizontal wind profiles could be calculated at the beginning and end of the hour period. Figure 2 shows sample spectra when the radar was pointed east and north, and the variation in mean wind with height is evident in the spectral displacements at 1500 m and 3000 m in the east-pointing mode. Positive velocities represent motion toward the radar. The velocity scale is radial velocity and has not been translated into the horizontal plane (by dividing by sin15°). To remove the primary effect of sidelobe clutter from stationary targets producing return at zero velocity, the spectra were interpolated across the zero ordinate to produce a flat segment there. The spectra are plotted in decibels of power vs. velocity, but the power scale is arbitrary because the computer graphics automatically scale each spectrum individually. However, the signal-to-noise ratio of the backscattered power can be judged qualitatively from the magnitude of the noise excursions far from the signal. If the signal is strong the noise fluctuations will be scaled to very small values.

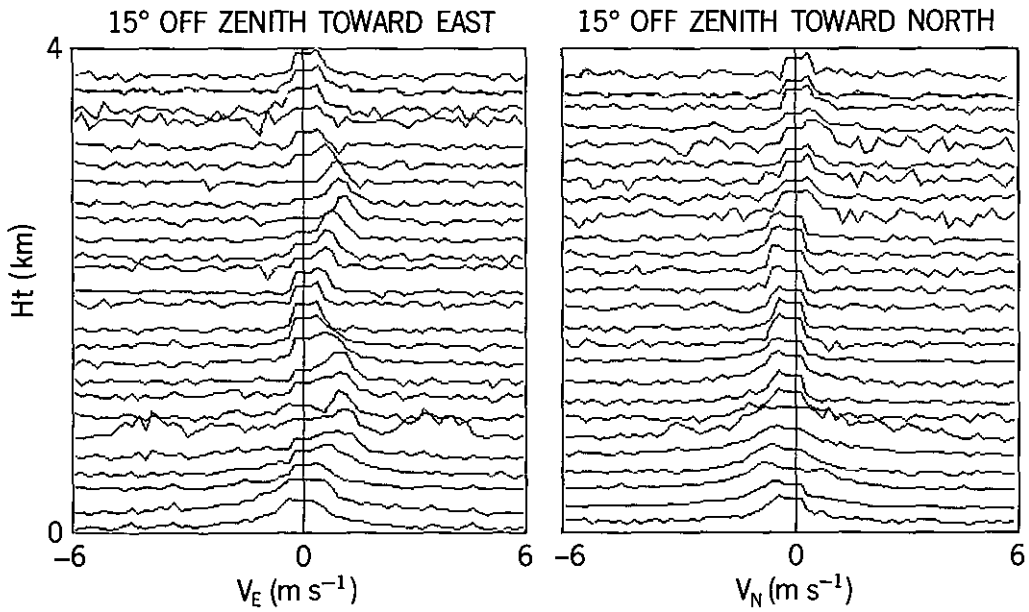

Figure 2. Sample spectra of power (on log scale) for radial velocities in 26 range gates. Antenna is pointing east and north, 15° off zenith. The 26th (top) range gate corresponds to an altitude of about 4 km. The ordinate scale is arbitrary because the computer scales each plot individually.

Figure 3 is a height-vs.-intensity plot of backscattered power (dB). All such plots of backscattered power show strong returns at 1 km range from traffic on highway Interstate 70. They also commonly show strong returns from point targets (birds and insects) throughout the lowest 2 km.

Figure 3 reveals that the height of the temperature inversion coincided with the strong backscattered power echo obtained from the radar at 1200 GMT. The presence of this elevated layer may be noted in the C_ϕ^2 and ε profiles in Fig. 4 (top frame) and the ratio profiles of $C_\phi^2/\varepsilon^{2/3}$ in Fig. 4 (bottom frame), where C_ϕ^2 and ε were calculated from (37) and (38). Figure 5 is a sample of five consecutive height profiles of raw Doppler spectra of vertical velocity. The narrow spectrum with strong signal around range gates 17 through 19 (corresponding to a height of 2.7 km to 3 km) coincides with the elevated stable layer.

The comparisons between the model estimates of C_ϕ^2 and ε and the radar measurements for this case are shown in Fig. 6. The balloon carrying the raob instrument was launched at 1110 GMT, and reached a height 4 km above the ground at 1121 GMT. The radar began operating in its high-resolution mode at 1200 GMT. We used the first 16 radar profiles closest in time to the balloon data to construct the figures.

In Fig. 6, we shifted the height of the model profiles (labeled on the right-hand side of the figures) relative to the radar measurements by about two range gates to match the height of the major feature of the profile. This assumes that the layer rose by about 300 m in the hour between the balloon launch and the radar measurements. Height changes of this order are not unusual. Note the gap in both model profiles between 2.4 and 2.7 km height where the balloon passed through a convective region. The radar data also show the strong clutter echoes near 1 km discussed in Sec. 3.2.1. As in the following cases, the agreement between the data and model C_ϕ^2 (Fig. 6a) is excellent in both shape and magnitude. However, the shapes of the measured and modeled ε profiles (Fig. 6b) are quite different.

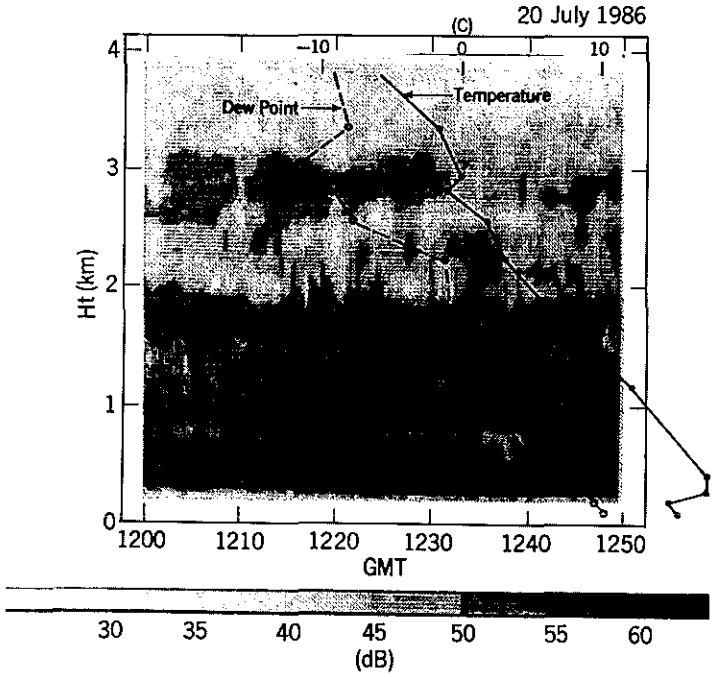

Figure 3. Intensity of received power (dB) vs. time and height. Power values are relative. The 1200 UT (GMT) raob soundings of temperature and dew point are superimposed. Note stable layer at about 3 km.

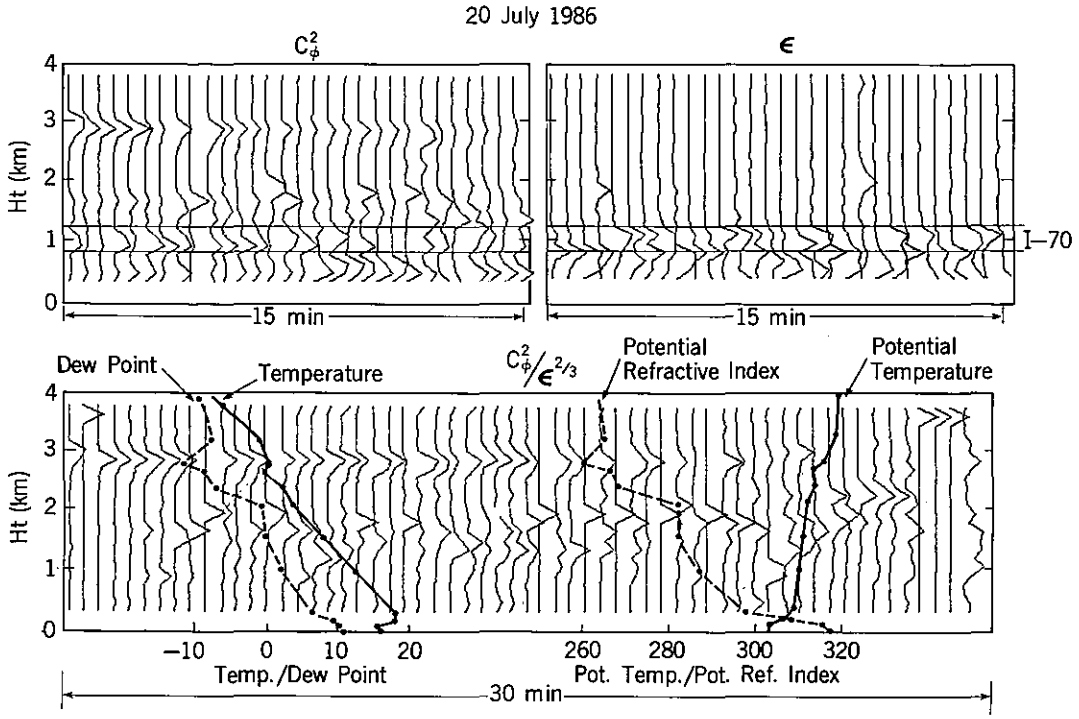

Figure 4. (Top) Sample side-by-side profiles of C_ϕ^2 and ε, and (bottom) profiles of the ratio $C_\phi^2/\varepsilon^{2/3}$. The contribution of traffic on Interstate 70 is mostly removed by taking the ratio. In side-by-side profiles the horizontal scale is arbitrary because the computer scales each profile individually. The raob values of temperature, dew point, potential temperature, and potential refractive index are superimposed on the bottom frame.

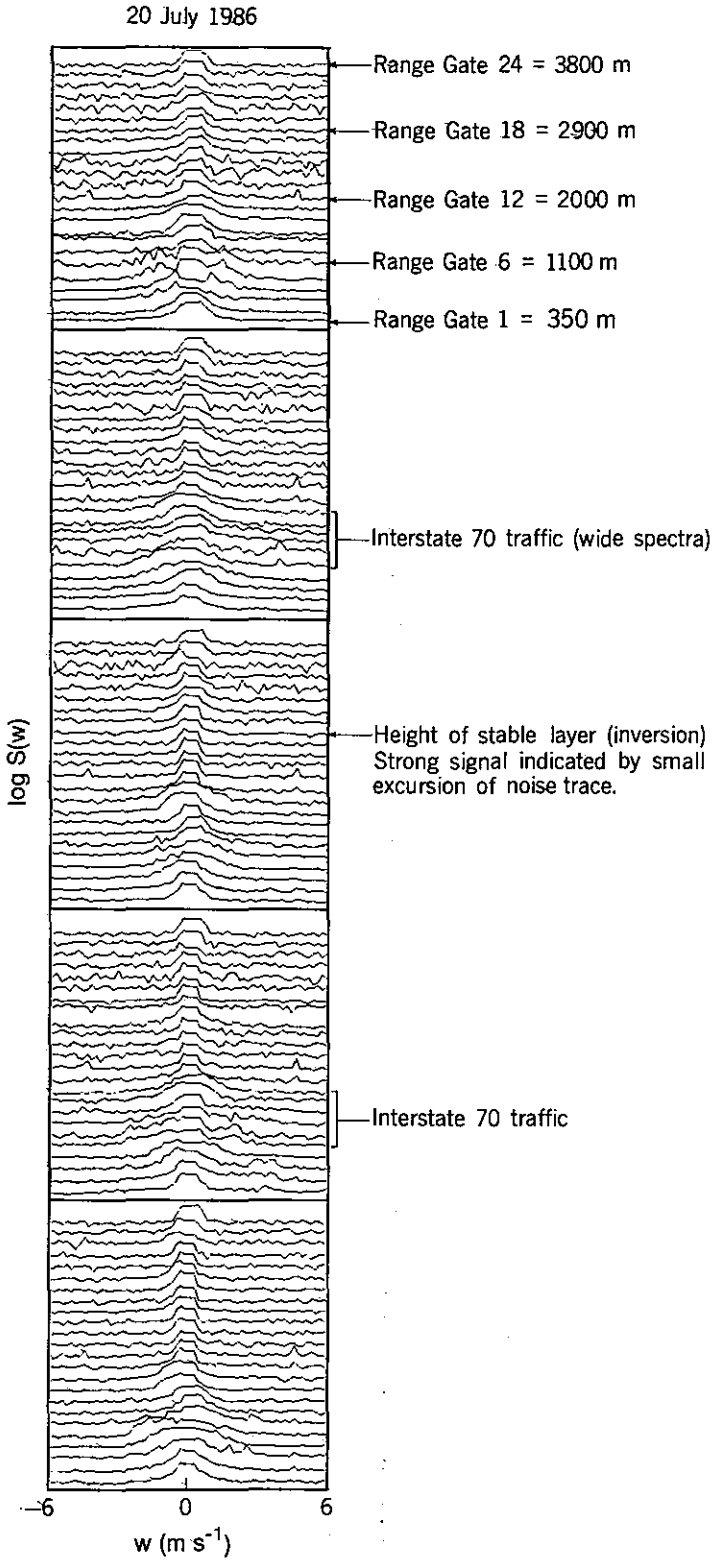

Figure 5. Sample of five successive spectral scans in the vertically pointing mode, illustrating the effect of the stable layer and I–70 traffic on spectral width.

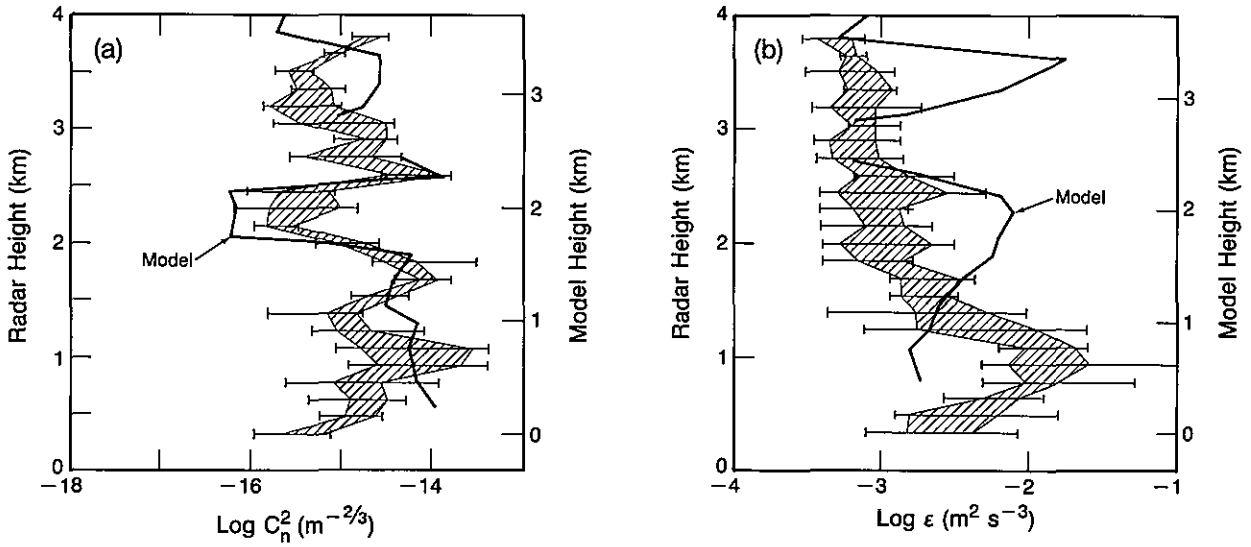

Figure 6. Height profiles of (a) $C_n^2 = C_\phi^2$ and (b) ε for 20 July 1986. The Stapleton radar began operating in the high-resolution mode at 1200 GMT. A profile was obtained every 30 s; data from the first 16 profiles are used in the figure. The horizontal bars at the height of the center of each range gate mark the extreme values of the data set. The shaded area encloses values in the middle quartiles, that is, half the data. The solid dark line is the model profile derived from the raob data; the balloon was launched from Stapleton at 1110 GMT.

3.2.2 24 June 1986

Figure 7 shows the presence of a strong humidity gradient around 3 km as may be noted from the dew point profile obtained from the raob around 1200 GMT on 24 June 1986. The height of the humidity gradient coincides with the strong backscattered power echo obtained from the radar. The strong return around 1 km is due to the clutter from traffic movement on the highway Interstate 70 (I–70).

The structure function parameter C_ϕ^2 was calculated from the backscattered power [Eq. (37)]. The Doppler spectral width was used to obtain eddy dissipation rate ε from the method of Frisch and Clifford (1974) [see (38)]. Figure 8 (top frame) shows sample profiles of C_ϕ^2. The profiles clearly indicate the presence of an elevated layer around 3 km, coinciding with the height of the strong humidity gradient obtained from the raob. The strong echo around 1 km is again due to ground clutter from highway I–70. The scattered returns between 1.5 and 2 km are probably due to the movement of birds. The bottom frame of Fig. 8 shows profiles of the ratio $C_\phi^2/\varepsilon^{2/3}$. This ratio was used to retrieve the temperature gradient from the radar data, using (21). Profiles of this ratio clearly reveal the presence of an elevated layer around 3 km, and the ratio also partially removes some types of clutter such as that from I–70 near 1 km.

Figure 9 shows a Doppler spectral display, for all 24 range gates, on 24 June 1986. The spectral broadening around range gates 5 through 7 is due to movement of traffic on I–70. The spectrum around range gates 18 and 19 indicates a clear-air event that corresponds to the height of the strong humidity gradient noted on that day.

The WPL Stapleton radar measurements of C_ϕ^2 and ε are compared with the Aeronomy Laboratory's model estimates in Fig. 10. The balloon carrying the raob instrument was launched at 1100 GMT, and it reached 4 km height above the ground at about 1115 GMT. The radar began operating in its high-resolution mode at 1200 GMT. We used the first eight radar profiles closest in time to the balloon data to construct the figures.

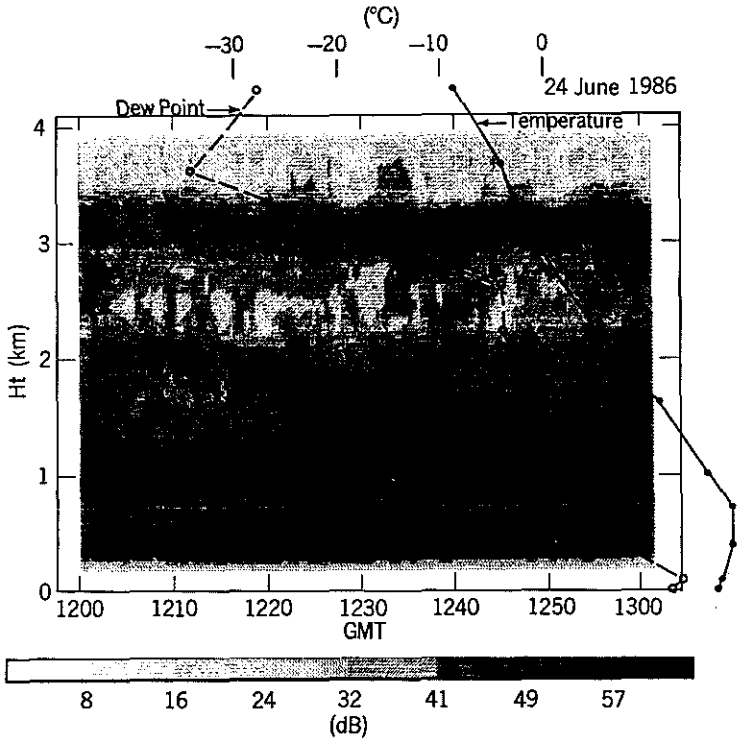

Figure 7. Time-height display of intensity of received power (dB) for 24 June 1986. Raob soundings for 1200 GMT are superimposed.

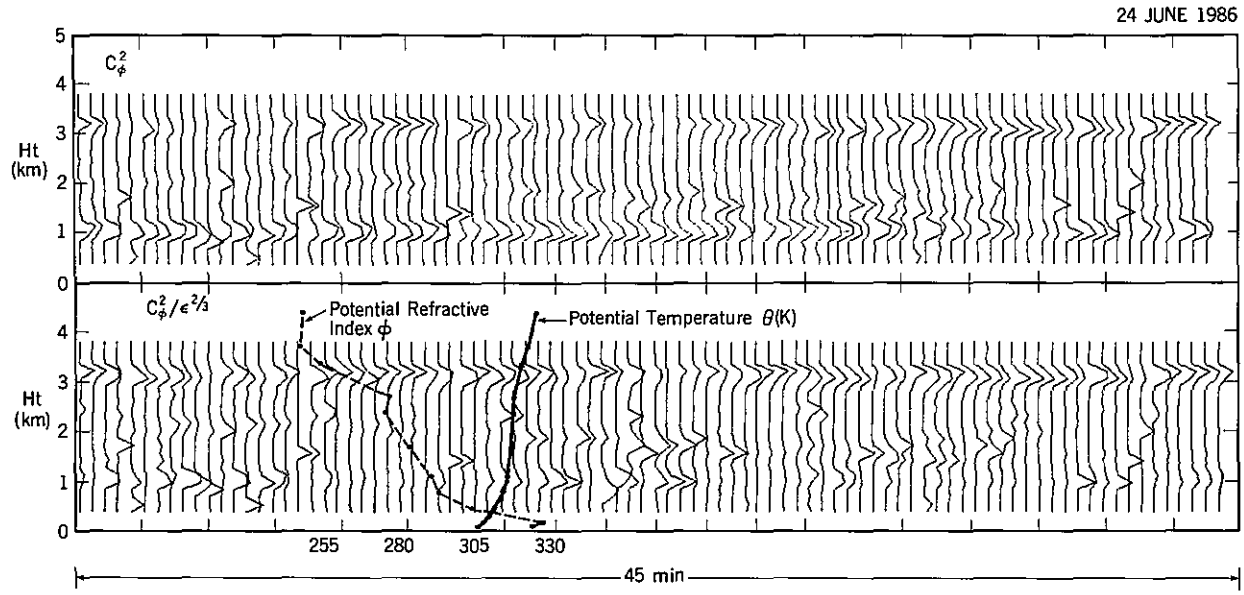

Figure 8. Side-by-side profiles of $C_\phi{}^2$ and $C_\phi{}^2/\varepsilon^{2/3}$ on 24 June. After most of the effect of I–70 has been removed by taking the ratio (lower frame), the remaining echoes, below the well-defined refractive layer, are more-or-less random in height and time and are mainly return from birds and/or insects.

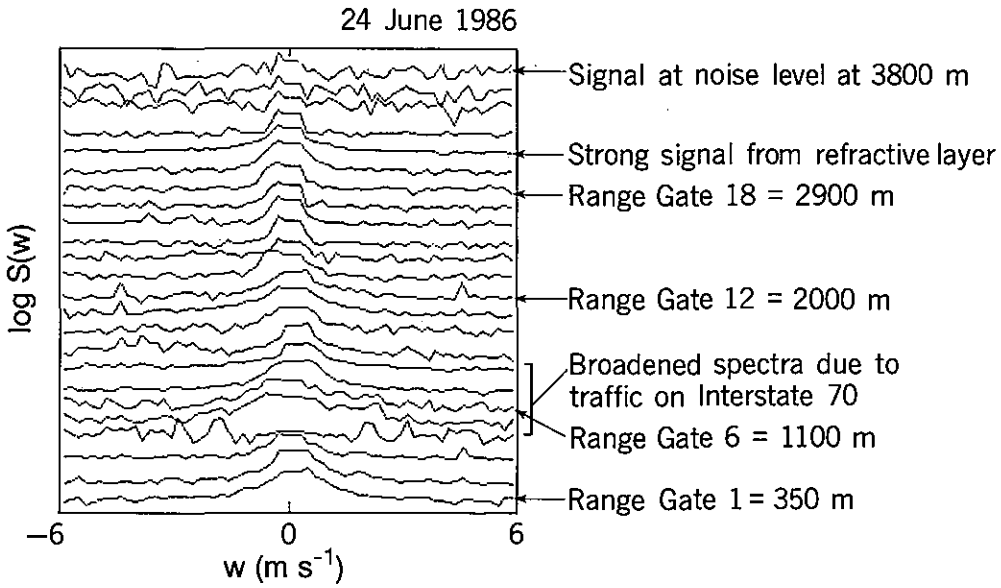

Figure 9. Sample of spectra of power (on log scale) on 24 June 1986.

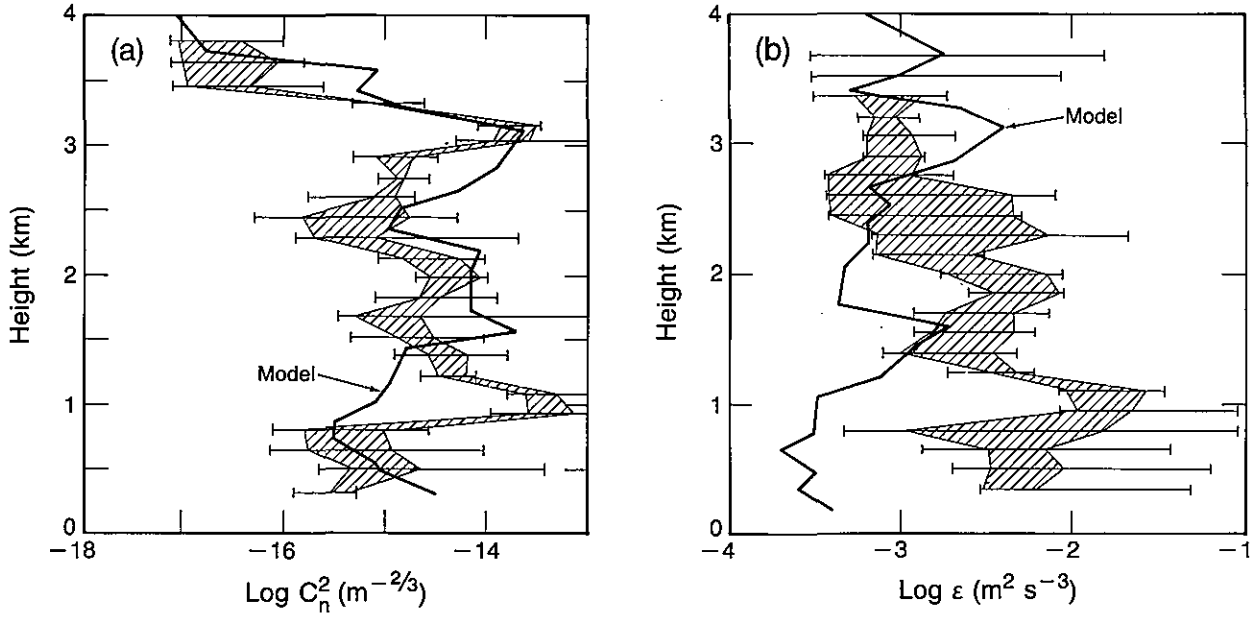

Figure 10. Height profiles of (a) $C_n^2 = C_\phi^2$ and (b) ε, as in Fig. 6 but for 24 June 1986.

Considering the hour difference in time between the balloon launch and the radar measurements, the agreement between the data and model C_ϕ^2 shown in Fig. 10a is excellent in both shape and magnitude. Both the model profile and the data show the strong humidity gradient layer around 3 km, and the measured profile again shows the strong clutter echoes near 1 km. The model profile fits even better if it is shifted down about one range gate, suggesting that the elevated layer may have risen about 150 m during the hour between 1100 and 1200 GMT. In contrast to the excellent agreement in the C_ϕ^2 profiles, the shapes of the measured and modeled ε profiles (Fig. 10b) are quite different, although their values, averaged over the profile, are similar.

3.2.3 24 September 1986

On 24 September 1986 a windstorm swept through Denver during the afternoon. On that day the radar was operating in its normal mode, switching through pulse lengths of 1 μs, 3 μs, and 9 μs in the east-, north-, and zenith-pointing modes. The temperature and dew point profiles obtained from the raob show the presence of temperature inversions at 2.4 km AGL and between 5 and 6 km AGL. The dew point depression indicates clouds between 4 and 5 km. The log C_ϕ^2 profiles on 24 September (Fig. 11) for the 1-μs and 3-μs pulse modes show strong returns near 2.4 km and between 5 and 6 km. The values of ε shown in Fig. 12, deduced from the 2nd moment of the Doppler spectrum, show the usual (e.g., Fig. 4b) strong average decrease with height. The maximum values of the ratio $C_\phi^2/\varepsilon^{2/3}$, calculated from the radar data obtained on 24 September 1986, are shown in Fig. 13 for the medium-altitude mode (3-μs pulse), and for the high-resolution, low-altitude mode (1-μs pulse). There were clouds between approximately 3 and 4.5 km AGL until about 2300 (GMT), resulting in very large values of the ratio in that time-height interval. However, clear-air conditions prevailed during the remainder of the record.

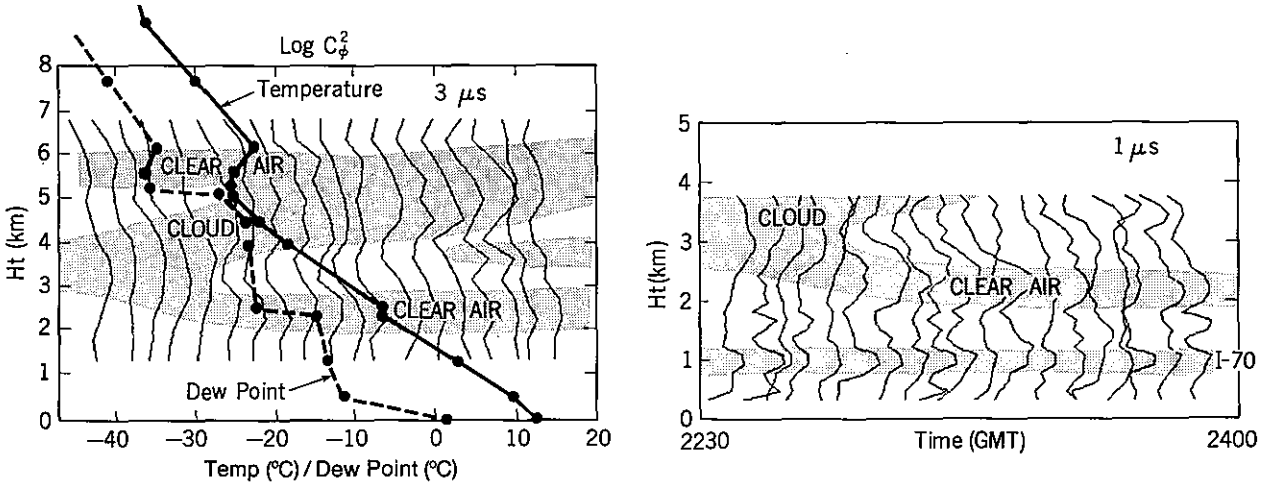

Figure 11. Side-by-side height profiles of log C_ϕ^2 for 3-μs pulse length (left) and 1-μs pulse length (right) on 24 September 1986. Raob sounding of 2400 GMT is superimposed on left frame and shows two strongly stable inversion layers. Stippled zones indicate layers of enhanced radar return. Clouds were present between 3 and 4.5 km until about 2300 GMT. Radar records were sampled in the vertical direction in each mode about every 5 s.

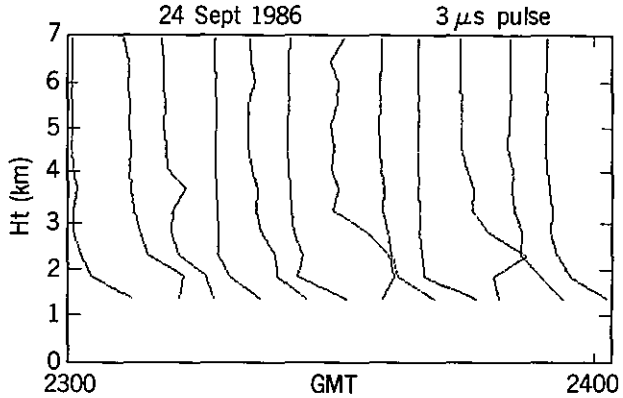

Figure 12. Sample side-by-side profiles of ε calculated from the width of the Doppler spectrum using (38). The horizontal scale is arbitrary.

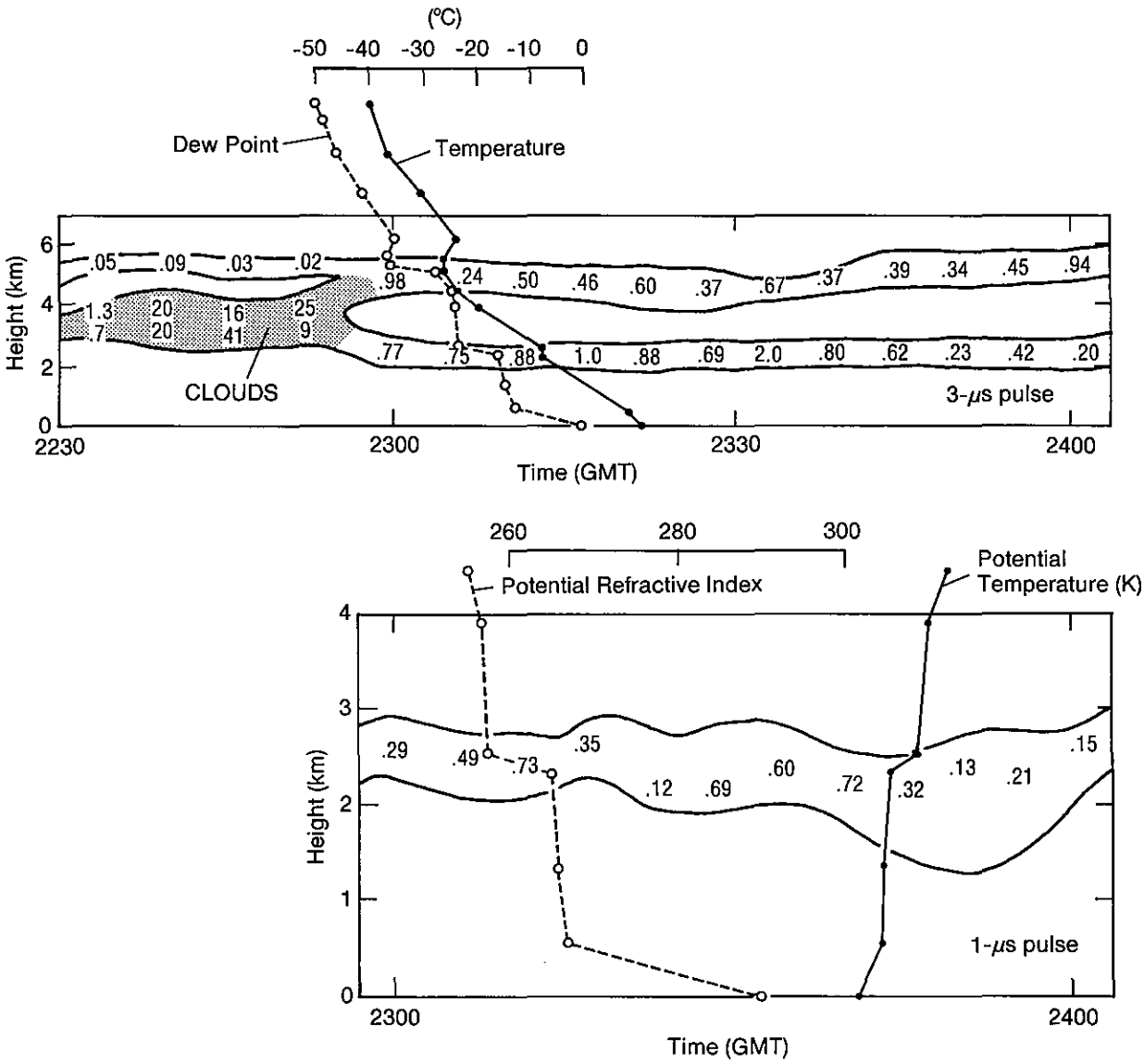

Figure 13. Maximum values of the ratio $C_\phi^2/\varepsilon^{2/3}$ near the centers of the layers shown in Fig. 12. Raob soundings of dew point and temperature are superimposed on the 3-μs pulse length record (top frame), and the corresponding profiles of potential refractive index and potential temperature are superimposed on the 1-μs pulse record (lower frame). Averages of the numerical values of the ratio were used to calculate the gradients listed in Table 2.

Comparisons between the model estimates of the structure function parameter C_ϕ^2 and ε and the Stapleton radar measurements are shown in Fig. 14. The balloon carrying that raob instrument was launched at 2301 GMT, and was 8 km above the ground at about 2330 GMT. Radar data from 2230 to 2356 GMT with a 3-μs pulse are included in the figures.

Figure 14a shows that, in the clear air above the cloud, the model C_ϕ^2 agrees well with radar measurements. Inside the cloud, however, the radar reflectivity increases dramatically as discussed above. In contrast to the good agreement between the C_ϕ^2 profiles, the shapes of the measured and modeled ε profiles (Fig. 14b) are quite different. In this case, however, the average ε of both the data and the model is about an order of magnitude larger than in the other two cases.

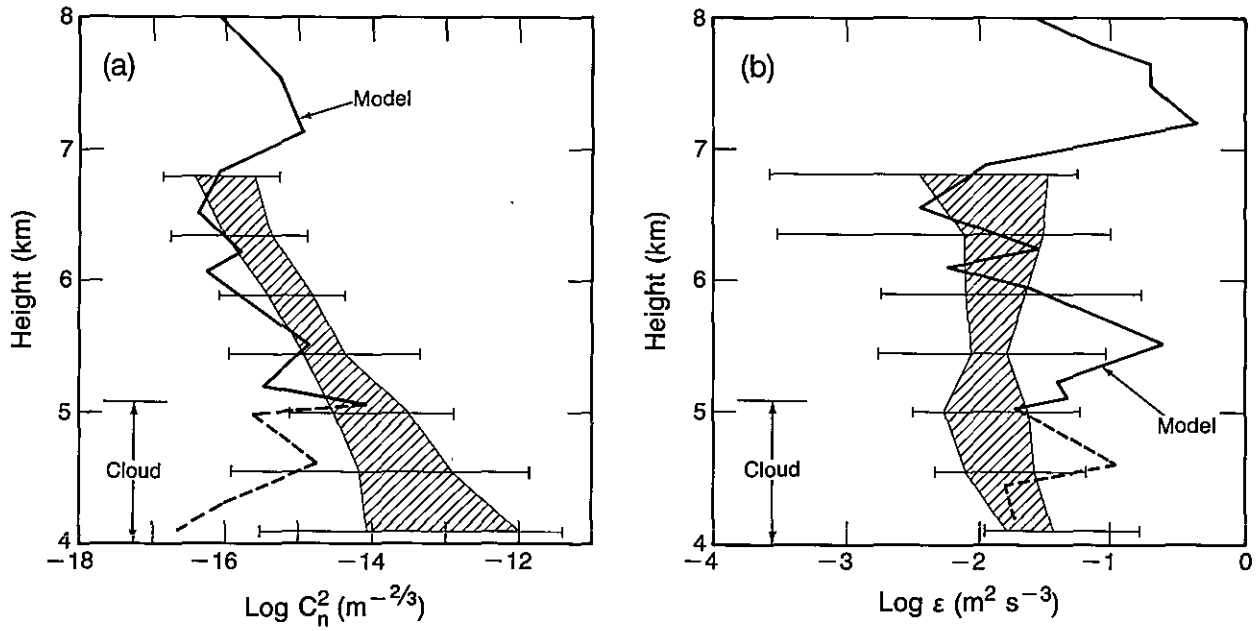

Figure 14. Height profiles of (a) $C_n^2 = C_\phi^2$ and (b) ε for 24 September 1986. The Stapleton radar was operated in mode 2 (see Table 1). A profile was obtained every 4.5 min; data from 2230 to 2356 GMT are included in the figure. The horizontal bars, located at the height of the center of each range gate, are the extreme values. The shaded area encloses half the measured values. The solid dark line is the model profile derived from the raob data; the balloon was launched from Stapleton at 2301 GMT.

3.3 The Effect of Clouds

In the course of our experiment the Stapleton radar detected stratiform clouds and fair weather convective cloud layers with droplets having very small fall velocities, suggesting mass median drop sizes as small as 100 μm. The plot of backscattered power in Fig. 15 illustrates cloud return recorded on the radar and the potential for serious "false alarms" from clouds in the radar detection of clear-air layers. The echoes above 3 km and the layer at 2 km are both from cloud. The upper echo shows an obvious fall velocity that is even more clearly defined in the reflectivity factor (Z) profiles of Fig. 16. The Doppler spectra in Fig. 17 show a distinct separation of the peaks due to clear air and to clouds, especially for the layer >3 km. The surface observations merely reported scattered clouds at about 2.5 km and broken clouds at a measured height at 3.1 km. The radar-measured fall velocity in the upper cloud was about 1.3 m s^{-1}, which gives a drop size of about 300 μm, on the basis of the Gunn-Kinzer relation between drop size and fall velocity. The fall velocity peak at 2 km (the 11th and 12th range gate spectra) is barely distinguishable from the clear-air return. It suggests a fall velocity of about 0.3 m s^{-1} relative to the clear-air motion, yielding a drop size of about 50 μm. It is notable that the spectral return from drops is separable from the clear air return, even for 50-μm drops. Thus the clear-air peak serves as an indicator of air movement, and the drop fall velocity spectrum relative to the clear air may be found.

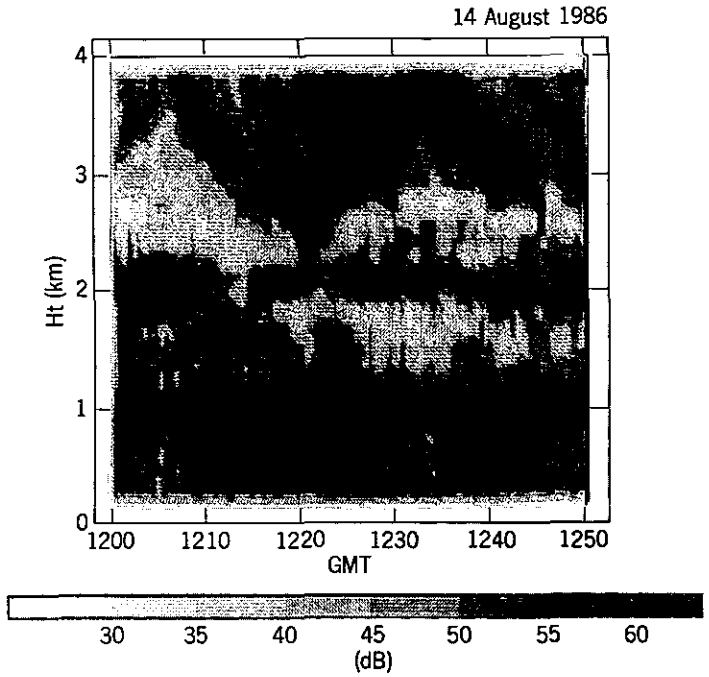

Figure 15. Time-height display of intensity of backscattered power (dB) for a case when cloud layers were present.

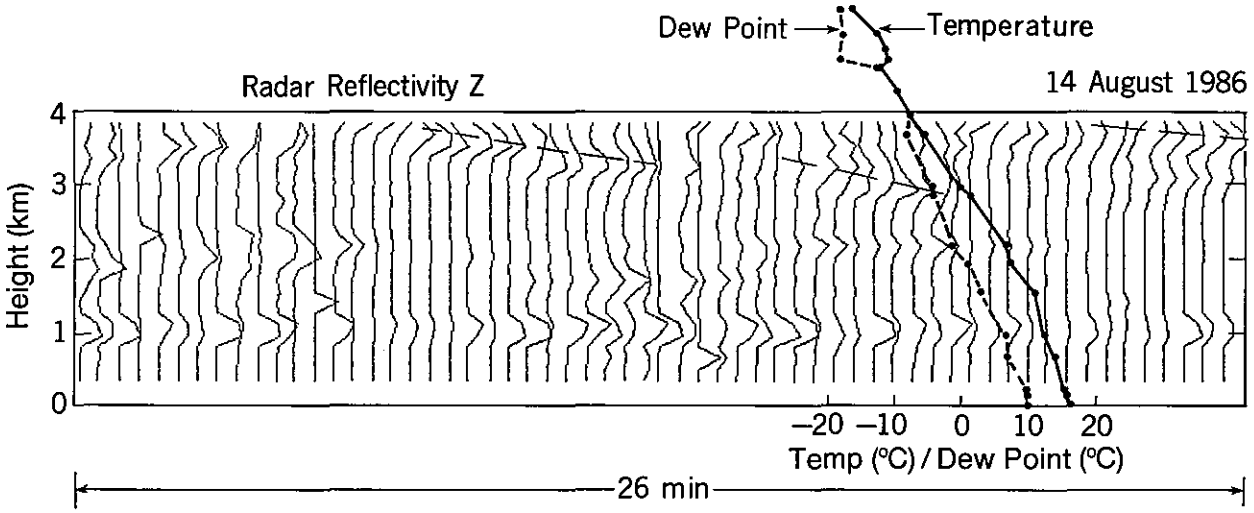

Figure 16. Side-by-side profiles of radar reflectivity for the case with cloud return shown in Fig. 15. These computer plots are scaled individually by the computer graphics, so the scale for each profile is relative only, and may be interpreted as C_ϕ^2 in the clear air and as Z within clouds. Note rate of fall of particles within the virga, indicated by the slope of the dashed lines. Dew point and temperature from the raob data are superimposed.

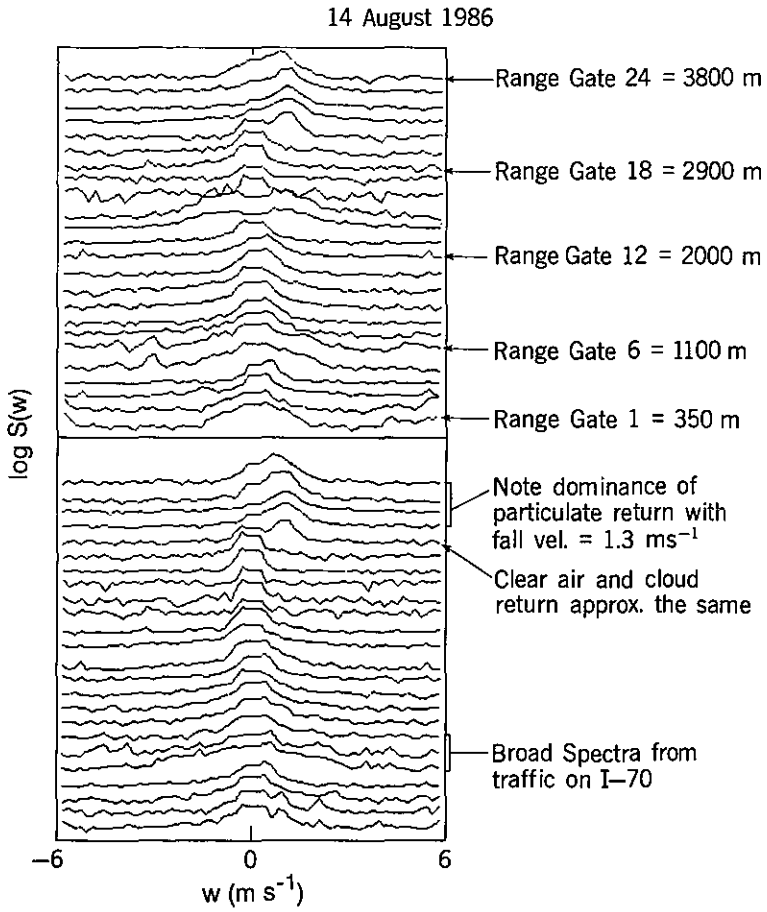

Figure 17. Sample of power spectra (on log scale) corresponding to data shown in Figs. 15 and 16. Note separation of the spectral peaks due to clear-air return, and the peaks due to falling drops at height above 3000 m. The indicated fall velocity of the drops agrees with the slope of the dashed lines in Fig. 16.

4. CONCLUSIONS

Under clear-air conditions, values of refractive index and/or temperature gradient could in theory be calculated from the ratio $C_\phi^2/\varepsilon^{2/3}$ [see (21)] if the mean gradient of (say) temperature, in the refractive index calculation, or of humidity, in the temperature calculation, could be estimated from an independent source such as synoptic weather analysis, radiometric retrieval, or an earlier raob. Table 2 shows the values of refractive index and temperature gradients obtained from radar measurements of C_ϕ^2 and ε, calculated using the raob values for the needed a priori temperature and humidity gradients. The resulting retrievals of refractive index and temperature gradient from the Stapleton radar yielded gradients of the same order as those measured by the raob (Table 2). However, the present experiment has revealed that the UHF wind-profiling radar at Stapleton is quite sensitive to nonprecipitating clouds even at these fairly long wavelengths (32 cm) and so would be subject to "false alarms" from cloud return. Insects and birds are also important sources of natural clutter. The clutter due to returns from traffic on highway I–70 was found to dominate the radar echoes in the crucial height range of 0–2 km where most of the temperature inversion layers are observed.

Table 2. — Calculated refractive index and temperature gradients from radar measurements of C_ϕ^2

Date	Calc. $d\phi/dz$	Meas. $d\phi/dz$	Calc. $d\theta/dz$	Meas. $d\theta/dz$
24 June	−0.057	−0.030	0.001	0.005
20 July	−0.038	−0.048	0.031	0.020
24 September				
3-μs pulse				
Upper layer	−0.018	−0.012	0.025	0.019
Lower layer	−0.018	−0.036	0.038	0.014
1-μs pulse				
Lower layer	−0.013	−0.036	0.068	0.014

The calculated refractive index gradients agree with the observed values better than the calculated temperature gradients agree with the measured temperature gradients. This may be attributed to the fact that radars measure C_ϕ^2 rather than C_θ^2.

The values of the eddy dissipation rate calculated from spectral broadening are very large near highway I–70, owing to traffic movement. They may contaminate the measured values for the lower layer on 24 September 1986, causing the substantial discrepancies between calculated and observed gradients.

In all the cases studied so far the modeled C_ϕ^2 profiles agree well in both magnitude and shape with the Stapleton 915-MHz radar measurements. In previous studies the Aeronomy Laboratory model was compared with the Sunset 40-MHz radar measurements. Note that the Stapleton and Sunset radars differ in the Bragg scattering scale by more than a factor of 20, and that the Sunset radar is located in a mountainous terrain in a region of often intense orthographic activity, whereas the Stapleton radar is located in the plains east of Denver.

The raob data used in the model comparisons with both the Stapleton and Sunset radars were obtained from the same Stapleton launch site. Because of the large distance (55 km) between the 40-MHz Sunset radar and the balloon launch site, data from many profiles were averaged together in the previous studies by Warnock et al. (1985, 1986). On the average, good agreement was found between the 40-MHz radar and the model. The comparisons included a calibration of the model to the 40-MHz Sunset measurements. However, the model calibration was not changed between the previous studies and this study, and identical values of all the model constants and parameters were used in all the studies. Thus, the good agreement found between the model and both radars has several important implications:

(1) The model and both radars are well calibrated.
(2) The model estimates C_ϕ^2 correctly for Bragg scattering scales over a range of 0.164 to 3.7 m.
(3) Because the model C_ϕ^2 values are very sensitive to the parameters of the vertical structure, this agreement implies that the fine structure is similar in the mountains and on the plains near Stapleton airport.
(4) The detailed agreement between the model and radar C_ϕ^2 profiles improves as the separation between the balloon launch site and the radar decreases; the major structures of the C_ϕ^2 profile are estimated by the model to within a few hundred meters height when the launch site and radar are adjacent and the observing times are within an hour.

In contrast to the good agreement between the modeled and measured C_ϕ^2, the measured and modeled ε profiles agree in magnitude but not in shape. The data profiles are smooth, whereas the model profiles display considerable structure similar in shape to the wind shear profiles.

ACKNOWLEDGMENTS

The authors wish to express their appreciation for indispensable assistance from Robert Weber and David Merritt, who provided basic software and radar data; Debbie Troxel for much assistance in the software, especially the gray-scale plots; David McLeod and Leslie Whittenmeir for advice and help in software development; and Martin Decker for advice and aid in acquiring raob data. We also acknowledge support from the National Science Foundation for one of us (N.S.) and from the Naval Ocean Systems Center, J. H. Richter, for partial support of one of us (E.E.G.).

REFERENCES

Bean, B. R., and E. J. Dutton, 1966: *Radio Meteorology*. National Bureau of Standards Monograph 92, 435 pp.

Beckmann, P., 1967: *Probability in Communication Engineering*. Harcourt, Brace and World, New York, 122–123.

Chadwick, R. B., K. P. Moran, R. G. Strauch, G. E. Morrison, and W. C. Campbell, 1976: Microwave radar wind measurements in the clear air. *Radio Sci.*, **11**, 795–802.

Clark, W. L., J. L. Green, and J. M. Warnock, 1985: Estimating meteorological wind vector components from monostatic Doppler radar measurements: A case study. *Radio Sci.*, **20**, 1207–1213.

Corrsin, S., 1951: On the spectrum of isotropic temperature fluctuations in an isotropic turbulence. *J. Appl. Phys.*, **22**, 417–423.

Doviak, R. J., and D. S. Zrnic, 1984: *Doppler Radar and Weather Observations*. Academic Press, London, 458 pp.

Frisch, A. S., and S. F. Clifford, 1974: A study of convection capped by a stable layer using Doppler radar and acoustic echo sounders. *J. Atmos. Sci.*, **31**, 1622–1628.

Fukao, S., T. Sato, N. Yamasaki, R. M. Harper, and S. Kato, 1982: Winds measured by a UHF Doppler radar and rawinsondes: Comparisons made on twenty-six days (August–September 1977) at Arecibo, Puerto Rico. *J. Appl. Meteorol.*, **21**, 1357–1363.

Gage, K. S., T. E. VanZandt, and J. L. Green, 1978: Vertical profiles of C_n^2 in the free atmosphere: Comparison of model calculations with observations. Proceedings, 18th Conference on Radar Meteorology, Mar. 28–31, Atlanta, GA, American Meteorological Society, Boston, 80–87.

Gage, K. S., J. L. Green, and T. E. VanZandt, 1980: Use of Doppler radar for the observation of atmospheric turbulence parameters from the intensity of clear air echoes. *Radio Sci.*, **15**, 407–416.

Gossard, E. E., and A. S. Frisch, 1987: The relationship of the variances of temperature and velocity to atmospheric static stability — application to radar and acoustic sounding. (Accepted, *J. Clim. Appl. Meteorol.*, 1987).

Gossard, E. E., and R. G. Strauch, 1983: *Radar Observations of Clear Air and Clouds*, Elsevier, Amsterdam, 280 pp.

Gossard, E. E., R. B. Chadwick, W. D. Neff, and K. P. Moran, 1982: The use of ground-based Doppler radars to measure gradients, fluxes and structure parameters in elevated layers. *J. Appl. Meteorol.*, **21**, 211–226.

Gossard, E. E., R. B. Chadwick, T. R. Detman, and J. Gaynor, 1984: Capability of surface-based, clear-air Doppler radar for monitoring meteorological structure of elevated layers. *J. Clim. Appl. Meteor.*, **23**, 474–490.

Green, J. L., J. M. Warnock, R. H. Winkler, and T. E. VanZandt, 1975: Studies of winds in the upper troposphere with a sensitive VHF radar. *Geophys. Res. Lett.*, **2**, 19–21.

Harper, R. M., and W. E. Gordon, 1980: A review of radar studies of the middle atmosphere. *Radio Sci.*, **15**, 195–209.

James, P. K., 1980: A review of radar observations of the troposphere in clear air conditions. *Radio Sci.*, **15**, 157–175.

Lumley, J. L., and H. A. Panofsky, 1964: *The Structure of Atmospheric Turbulence*. Wiley, New York, 239 pp.

Ottersten, H., 1969: Mean vertical gradient of potential refractive index in turbulent mixing and radar detection of CAT. *Radio Sci.*, **4**, 1247–1249.

Strauch, R. G., D. A. Merritt, K. P. Moran, K. B. Earnshaw, and D. van de Kamp, 1984: The Colorado wind-profiling network. *J. Atmos. Ocean. Tech.*, **1**, 37–49.

Strauch, R. G., A. S. Frisch, D. A. Merritt, K. P. Moran, B. L. Weber, and D. C. Welsh, 1987: The precision and accuracy of radar measurements. *J. Atmos. Ocean. Tech.* (in press).

Tatarskii, V. I., 1971: *The Effects of the Turbulent Atmosphere on Wave Propagation*. U.S. Dept. of Commerce, National Technical Information Service, Springfield, VA [N72–18163].

VanZandt, T. E., J. L. Green, K. S. Gage, and W. L. Clark, 1978: Vertical profiles of refractivity turbulence structure constant: Comparison of observations by the Sunset radar with a new theoretical model. *Radio Sci.*, **13**, 819–829.

VanZandt, T. E., K. S. Gage, and J. M. Warnock, 1981: An improved model for the calculation of profiles of C_n^2 and ε in the free atmosphere from background profiles of wind, temperature, and humidity. Proceedings, 20th Conference on Radar Meteorology, Nov. 30–Dec. 3, 1981, American Meteorological Society, Boston, MA, 129–135.

Warnock, J. M., and T. E. VanZandt, 1985: A statistical model to estimate the refractivity turbulence structure constant C_n^2 in the free atmosphere. NOAA TM ERL AL–10, NOAA Environmental Research Laboratories, Boulder, CO, 175 pp.

Warnock, J. M., T. E. VanZandt, J. L. Green, and R. H. Winkler, 1978: Comparison between wind profiles measured by Doppler radar and by rawinsonde balloons. *Geophys. Res. Lett.*, **5**, 109–112.

Warnock, J. M., T. E. VanZandt, and J. L. Green, 1985: A statistical model to estimate mean values of parameters of turbulence in the free atmosphere. Preprints, Seventh Symposium on Turbulence and Diffusion, November 12–15, 1985, Boulder, CO, American Meteorological Society, Boston, MA, 156–159.

Warnock, J. M., J. L. Green, and W. L. Clark, 1986: Studies of C_n^2 and its variability measured by the Sunset clear-air radar. Preprints, 23rd Conference on Radar Meteorology, September 22–26, 1986, Snowmass, CO, American Meteorological Society, Boston, MA, 34–37.

☆ U.S. GOVERNMENT PRINTING OFFICE: 1987—573-002/80,505